Measurement of Nanometric Heights by Modal Decomposition

Valeria Rodríguez-Fajardo[†] and Andrew Forbes[*]
School of Physics, University of the Witwatersrand, Private Bag 3, Johannesburg 2050, South Africa

(Received 26 August 2022; revised 14 November 2022; accepted 22 November 2022; published 22 December 2022)

Measuring the height of steplike features in samples has become important in many scientific and industrial applications. It is routinely done using both tactile and optical methods, the latter being preferable due to their noncontact nature and improved speed capabilities. Nevertheless, techniques less sensitive to instabilities or without calibration or reference sample requirements would be advantageous. Here, we propose a method to measure nanometric step heights based on a modal analysis of the reflected or transmitted field. Our approach requires a minimum of four single-point measurements by detectors with no spatial resolution (photodiodes) and yet can reconstruct spatial structure with nanometric resolution. It has the benefits of not requiring a reference measurement or calibration and it is completely digital, thus offering high reliability and real-time measurement. As proof of principle, we perform measurements on reflective samples, finding excellent agreement between the set and measured values, with uncertainties comparable to those of scanning-force microscopes.

DOI: 10.1103/PhysRevApplied.18.064068

I. INTRODUCTION

Surface metrology has become vital in many industrial and scientific applications [1]. In particular, measuring the height of steplike features is crucial in areas such as evaluation of nanomanufacturing [2] and calibration of vertical standards [3,4]. Optical methods are in general preferable to tactile techniques [5–9] due to their noncontact nature and improved speed [10–13]; therefore there has been substantial interest in their development. Approaches include two-wavelength phase-shifting interferometry [14], chromatic confocal microscopy [15], phase-measuring deflectometry [16,17], and digital holographic microscopy [18, 19]. Despite their proved advantages, the performance of optical methods is in general affected by instabilities in the system [20] caused, e.g., by vibrations and, in the case of reflective samples, they usually require a reference optical flat, thus hindering their potential. The use of structured light [21], in which one or more of the degrees of freedom of light are exploited, offers the possibility of overcoming these drawbacks. Such is the case of mode projection [22], which offers improved robustness against vibrations although at the cost of requiring a reference measurement, and coherent Fourier scatterometry with singular beams [23], which has recently been proposed. The use of light with orbital angular momentum for so-called spiral imaging has been proposed [24] and experimentally exploited for measuring phase jumps [25] and has proven highly versatile, for example, in edge enhancement of objects [26].

Here, we present a technique capable of measuring the height of a step in samples in the nanometric regime. We show that the spatial-mode content of the reflected or transmitted light from a sample holds all the required information to infer the sample structure. This is in contrast to other optical techniques that often rely on interference fringes as the sole information carried by the field of the sample. Our method, which requires a spatial-mode decomposition of the resulting light into some basis, is completely digital, utilizes a single laser beam, and does not require a reference measurement or calibration. It therefore offers improved reliability and robustness against vibrations. In our experimental implementation, we demonstrate its performance on an artificial sample programmed on a spatial light modulator, since it provides a versatile platform for our proof-of-principle measurements and it allows predetermined step heights to be programmed. We find excellent agreement between the set and measured heights, validating the approach.

II. CONCEPT

Modal decomposition is a well-known technique [27], in which a light beam is expressed as a superposition of modes of a chosen basis. The latter is comprised of a series of orthogonal light modes and must be complete, thus ensuring that a field can be expanded as a linear combination of them. The coefficients in this expansion are in general complex, with their magnitude correlating the beam to each of the specific modes in the basis

[*]andrew.forbes@wits.ac.za
[†]now at Department of Physics and Astronomy, Colgate University, Hamilton, New York 13346, USA

and the phase accounting for possible intermodal phases. The crucial advantage is that, given a specific basis, the knowledge of the coefficients is enough to completely describe the properties of the field. The process of modal decomposition therefore reduces to a measurement of these coefficients.

Figure 1(a) illustrates the principle of modal decomposition using the Hermite-Gaussian (HG) [28] modes as the basis, where, for the sake of simplicity, we only make use of one of their indexes. The left-hand side represents the field of interest $U(\mathbf{r})$ (amplitude at the top, phase at the bottom), and the right-hand side each element in the basis (amplitude and phase) weighted by its corresponding coefficient $C_{j,0}$. Mathematically, this is equivalent to

$$U(\mathbf{r}) = \sum_{j,i=0}^{\infty} C_{j,i}\Psi_{j,i}(\mathbf{r}), \tag{1}$$

where $\Psi_{j,i}(\mathbf{r})$ represents the element (j,i) in the basis and the coefficients, by virtue of the orthogonality of the basis elements, can be determined from

$$C_{j,i} = \iint U(\mathbf{r})\Psi^*_{j,i}(\mathbf{r})d\mathbf{r}, \tag{2}$$

where $(\cdot)^*$ represents the complex conjugate. The interpretation of Eq. (2) is that each coefficient is the projection of the field onto the corresponding mode in the basis. Experimentally, we can measure these coefficients by taking advantage of the Fourier-transforming properties of lenses. Specifically, imaging a given field of interest $U(\mathbf{r})$ onto a correlation filter $\Psi^*_{j,i}(\mathbf{r})$ and subsequently Fourier transforming the result [Fig. 1(b)] yields [29]

$$W(\tilde{\mathbf{r}}) \propto \iint U(\mathbf{r})\ \Psi^*_{j,i}(\mathbf{r}) \exp\left(-i\,\frac{2\pi}{\lambda f}\,\tilde{\mathbf{r}}\cdot\mathbf{r}\right) d\mathbf{r}, \tag{3}$$

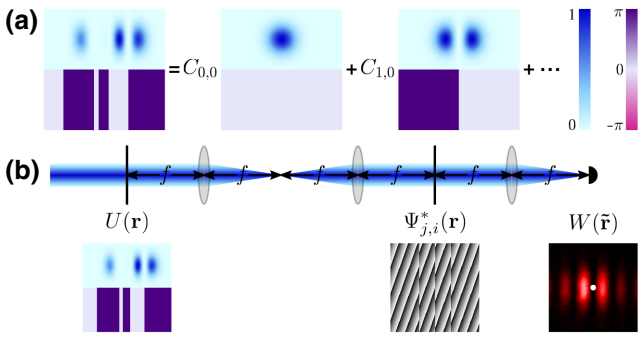

FIG. 1. (a) A modal-decomposition conceptual sketch using the HG modes as a basis. (b) A schematic of the measurement of the modal powers $|C_{j,i}|^2$ using the Fourier-transforming properties of a lens.

where f is the focal distance of the lens used. Evaluation of this expression at $\tilde{\mathbf{r}} = 0$ results in

$$W(0) \propto \iint U(\mathbf{r})\ \Psi^*_{j,i}(\mathbf{r})d\mathbf{r}, \tag{4}$$

which is proportional to the coefficient $C_{j,i}$ [Eq. (2)]. The intensity at the center of the beam is thus

$$|W(0)|^2 \propto |C_{j,i}|^2, \tag{5}$$

which represents the modal power of the corresponding coefficient and which we can easily measure using a camera or photodetector. Since the resolution of the optical system determines the physical size of $\tilde{\mathbf{r}} = 0$, $|C_{j,i}|^2$ is measured by integrating over a finite area [being the size of the sensor or a small circle in an image, as illustrated as a white point in the bottom-right inset of Fig. 1(b)]. Importantly, the filter can be implemented using a hologram displayed on a spatial light modulator, which has the added advantage of allowing us to change the filter as needed to determine all contributing coefficients.

It is often convenient to choose a basis that shares the same symmetry with the beam. For instance, for Cartesian coordinates, it is advantageous to use HG modes,

$$\psi_k(u) = \sqrt{\frac{2^{-(k-1/2)}}{\sqrt{\pi}\,w_0 k!}}H_k\left(\frac{\sqrt{2}u}{w_0}\right)\exp\left(-\frac{u^2}{w_0^2}\right), \tag{6}$$

where $H_k(u)$ is the Hermite function of order k and w_0 is the Gaussian beam width. Note that $\{\psi_k(u)\}_{k=0,1,2,\ldots}$ are orthonormal, i.e.,

$$\int_{-\infty}^{\infty} \psi_j(u)\psi_i(u)du = \delta_{j,i}, \tag{7}$$

and satisfy the parity relation $\psi_k(-u) = (-1)^k\psi_k(u)$.

Now, let us assume that a Gaussian beam $U_0(x,y)$ impinges on a reflective sample with a sharp straight discontinuity (a step) in its height [Fig. 2(a)]. As a result of this interaction, there will be a phase difference between the two halves of the beam that depends on the height of the step, h, as

$$\varphi_{\text{step}} = \frac{4\pi}{\lambda}h, \tag{8}$$

where λ is the wavelength and where we take into account that the side of the beam hitting the lower level travels twice the distance h in comparison to the one hitting the upper level. Thus the beam properties will be modified, the change being more prominent for higher steps, allowing us to quantify the height of the step by investigating the change in the beam features. Specifically, by taking advantage of the modal description of light beams, we propose

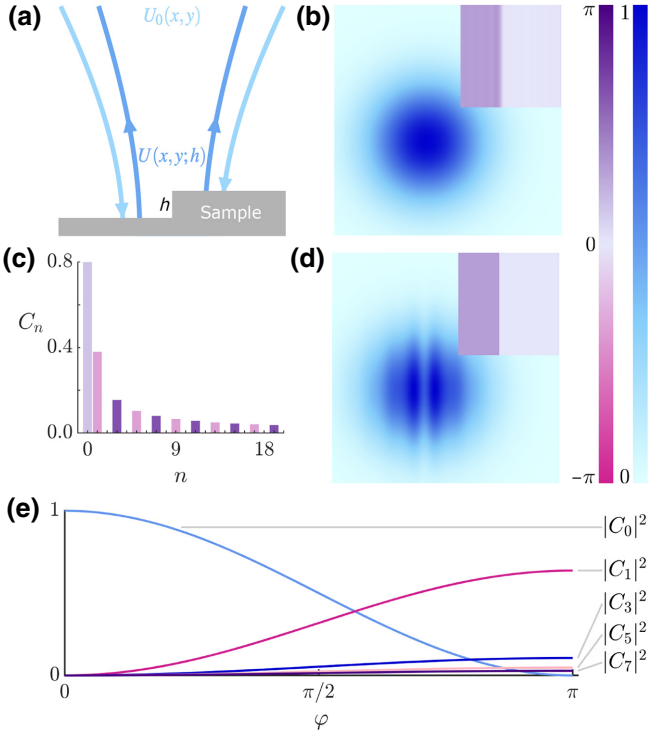

FIG. 2. (a) A schematic of the interaction of the light with the sample. An incoming beam $U_0(x,y)$ hits the step and is reflected back carrying information of the height h into the transformed field $U(x,y;h)$. (b) The intensity and phase (inset) of the analytical beam ($U(x,y;h)$) just after leaving the sample for a step with height 50 nm. (c) The amplitude (bar height) and phase (bar color) of the calculated decomposition coefficients and (d) the corresponding reconstructed field (intensity and phase) of the beam shown in (b). Note how all even coefficients vanish. (e) The modal power of the first nonzero coefficients as a function of the phase difference between the two halves of the beam. Note that all coefficients with odd $j \geq 1$ behave in the same manner, opposite to that with $j = 0$.

to infer the step height from the modal coefficients of the propagated beam.

Given the problem symmetry, we work in Cartesian coordinates, such that the y axis is located along the step, and decompose the resulting field U into HG modes. In this case, the electric field just after the sample can be expressed as the product of two functions, one for each coordinate, as $U(\mathbf{r};h) = U_x(x)U_y(y)$, with

$$U_x(x) = \psi_0(x)\begin{cases}\sqrt{R_1}\exp(i\varphi), & x < 0,\\ \sqrt{R_2}, & 0 \leq x,\end{cases}$$
$$U_y(y) = \psi_0(y), \tag{9}$$

where we assume that the center of the Gaussian beam hits the step precisely and we allow each side of the step to have a different reflectivity: R_1 and R_2 for $x < 0$ and $0 \leq x$, respectively. The phase term

$$\varphi = \varphi_{\mathrm{SLM}} + \frac{4\pi}{\lambda}h \tag{10}$$

is a scalar value that contains the information of the height of the step as well as an additional phase φ_{SLM} that we can control.

We want to decompose our field U [Eq. (9)] into HG modes, i.e.,

$$U(x,y) = \sum_{j=0}^{\infty}\sum_{i=0}^{\infty} C_{j,i}\psi_j(x)\psi_i(y), \tag{11}$$

the coefficients of which are determined from

$$C_{j,i} = \iint_{-\infty}^{\infty} U(x,y)\psi_j(x)\psi_i(y)dxdy, \tag{12}$$

which, given that $U(x,y)$ is separable, can be solved for each coordinate separately. On the one hand, since the HG modes are orthonormal [Eq. (7)], it is easy to see that the integral over y,

$$\int_{-\infty}^{\infty}\psi_0(y)\psi_i(y)dy = \delta_{0,i}, \tag{13}$$

vanishes for all $i > 0$ and is equal to 1 for $i = 0$; thus we can rewrite Eq. (11) as

$$U(x,y) = \sum_{j=0}^{\infty} C_j\psi_j(x)\psi_0(y). \tag{14}$$

On the other hand, the result of the integral over x of Eq. (12) is

$$C_j = \begin{cases}\frac{1}{2}\left(\sqrt{R_2} + \sqrt{R_1}e^{i\varphi}\right), & j = 0,\\ 0, & \text{even } j > 0,\\ \frac{(-1)^{j-1}/2(j-2)!!}{\sqrt{2\pi j!}}\left(\sqrt{R_2} - \sqrt{R_1}e^{i\varphi}\right), & \text{odd } j > 0,\end{cases} \tag{15}$$

where we use [30]

$$\int_0^u e^{-v^2}H_j(v)dv = H_{j-1}(0) - e^{-u^2}H_{j-1}(u) \tag{16}$$

and

$$H_j(0) = 0 \qquad \text{odd } j, \tag{17}$$
$$H_j(0) = (-1)^{j/2}2^{j/2}(j-1)!! \qquad \text{even } j, \tag{18}$$

in which $(\cdot)!!$ is the double factorial. Note how only the zeroth and odd coefficients contribute to the summation,

as expected because of the symmetry of the problem. Figure 2(b) presents the analytical electric field $U(x,y)$ calculated using Eq. (9) for a step with height 50 nm just after the impinging Gaussian beam has interacted with the sample. The effect is observed in the phase of the field, where there is a discontinuity along the step. The corresponding computed modal coefficients [Eq. (15)] and reconstructed field [Eq. (14)] are shown in Figs. 2(c) and 2(d), respectively, where it can be seen that the latter resembles the analytical field very closely, except along the step, since the amplitude of the field must vanish where there is a phase discontinuity.

We now focus our attention on the modal powers $|C_j|^2$, since in the laboratory we measure quantities proportional to them [27]. Figure 2(e) presents the power for the first five nonzero coefficients in the expansion. Note that all coefficients with odd n have the same dependence on the phase φ and only differ in their decreasing amplitude. Crucially, this behavior is opposite to that for $j = 0$, such that the power of the former increases with φ, whereas it decreases for the latter. Thus, since the two dominant coefficients are the zeroth and first ones, we use them to extract the information in which we are interested. From the expressions for these two coefficients, after some algebra, we find the relation

$$\frac{2|C_0|^2 - \pi|C_1|^2}{2|C_0|^2 + \pi|C_1|^2} = \frac{2\sqrt{R_1R_2}}{R_1 + R_2}\cos\left(\varphi_{\mathrm{SLM}} + \frac{4\pi}{\lambda}h\right), \quad (19)$$

which relates what we measure ($|C_0|^2$ and $|C_1|^2$) to the information that we want (R_1, R_2, and the step height h). Defining

$$y = \frac{2|C_0|^2 - \pi|C_1|^2}{2|C_0|^2 + \pi|C_1|^2},$$

$$A = \frac{2\sqrt{R_1R_2}}{R_1 + R_2},$$

$$B = \frac{4\pi}{\lambda}h, \quad (20)$$

Eq. 19 becomes

$$y = A\cos(\varphi_{\mathrm{SLM}} + B), \quad (21)$$

which we use as a fitting model with φ_{SLM} as the independent variable. We thus compute the step height from $h = (\lambda/4\pi)B$. Since B is limited to the interval $[0, 2\pi]$, the height cannot be directly determined beyond $\lambda/4$, which, interestingly, is the same limit found when following an interference approach [19].

III. EXPERIMENTAL DETAILS

We now describe the experimental implementation of our method [Fig. 3(a)]. Light coming out of a He-Ne laser ($\lambda = 632.8$ nm) is expanded and collimated by a telescope (lenses L_1 and L_2 with focal lengths $f_1 = 50$ mm and $f_2 = 500$ mm, respectively) and directed toward a liquid-crystal spatial light modulator (SLM_1, Holoeye Pluto 2, pixel pitch 8 μm). We create suitable holograms to mimic the effect of a sample with a step in height (the inset shows a representative example), allowing us to use the SLM as a highly versatile artificial sample. We then image the sample plane (SLM plane) onto a second SLM (SLM_2) by means of lenses L_3 ($f_3 = 750$ mm) and L_4 ($f_4 = 400$ mm) in a $4f$ configuration. We generate and display phase-only decomposition holograms (the particular case for C_3 is shown in the inset) as described in Ref. [27], to which we add an extra phase φ_{SLM} so that we obtain data of the form of Eq. (21). The beam is then relayed using an unitary magnification telescope (lenses L_5 and L_6 with focal

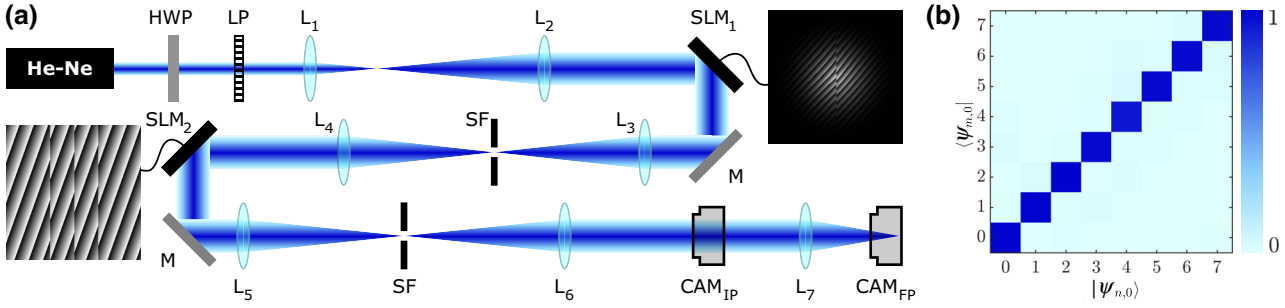

FIG. 3. (a) A schematic of the experimental setup. After being expanded and collimated, a He-Ne laser beam impinges onto a SLM, where a hologram representing an artificial sample is displayed. This plane is then relayed onto a second SLM, which performs a modal decomposition of the field. Proper alignment between the sample and the decomposing holograms is ensured by placing a camera on the image plane ($\mathrm{CAM_{IP}}$) and measurements are done at the Fourier plane ($\mathrm{CAM_{FP}}$). Spatial filters are used to reject unwanted diffraction orders and the power controlled by rotating a half-wave plate placed just before a linear polarizer. HWP, half-wave plate; LP, linear polarizer; L_i, lens; SLM_i, liquid-crystal spatial light modulator; M, mirror; SF, spatial filter; CAM, digital camera. (b) The measured crosstalk matrix of the optical system, showing its excellent performance since all off-diagonal elements are close to zero.

lengths $f_5 = f_6 = 150$ mm) and subsequently Fourier transformed by lens L_7 ($f_7 = 300$ mm). The beam power is controlled using a combination of a half-wave plate (HWP) and a linear polarizer (LP) oriented to transmit horizontally polarized light. Irises are placed at each of the Fourier planes of the SLMs to filter out diffraction orders different from the first one. Initially, a camera is placed at the image plane of the second SLM (CAM_{IP}) to ensure that the beam coming from the sample is properly centered with the decomposition hologram.

We generate holograms of the sample following a complex amplitude modulation approach [31], in which it is possible to simultaneously imprint phase and amplitude information into a beam using a phase-only hologram. Here, a desired scalar paraxial field $E(\mathbf{r}_\perp, z_0) = A(\mathbf{r}_\perp, z_0)\ \exp(i\Phi(\mathbf{r}_\perp, z_0))$ is encoded in the hologram via the phase profile $H(m,n) = M(m,n)\ \mathrm{Mod}\{F(m,n) + G(m,n), 2\pi\}$, with $M = 1 + 1/\pi \,\mathrm{sinc}^{-1}(A)$, $F = \Phi - \pi M$, and G and $M\{\cdot, 2\pi\}$ representing a grating phase profile and the 2π-modulo operation, respectively. Notably, since the sinc^{-1} function (the inverse function of the sinc) is not analytical, the method requires the use of a lookup table. We use a blazed grating $G(m,n) = 2\pi(\nu_n n + \nu_m m)$, where $\nu_{n,m}$ is the groove density in each direction, to separate the modulated light (in the first diffraction order) from unwanted light.

In our method, it is important to compensate for any wave-front distortions (aberrations) produced by the SLM or other optical elements in the setup. We follow the procedure proposed by Jesacher *et al.* [32], which is based on the Gerchberg-Saxton algorithm and requires only an image of a distorted vortex (OAM) beam at the Fourier plane. The resulting phase map serves as a correction matrix, which is stored and subtracted from any subsequent holograms.

Measurements of the modal powers are carried out from images acquired by a camera located at the Fourier plane (CAM_{FP}). In each case, the modal power is calculated by integrating the intensity within a circular area with a size according to the resolution of the optical setup, which depends on the beam size and the numerical aperture. In the experiment, for each decomposing mode, we use the complete phase-modulation range of the SLM, which is equivalent to amplitude-normalized decomposing modes. However, modes as defined in Eq. (6) are normalized to unitary power; thus it is necessary to calibrate the data using the known maximum amplitudes of the analytical modes.

The performance of the system is first verified by implementing a crosstalk-matrix measurement. Here, we sequentially display holograms corresponding to HG modes in the first SLM and decomposition holograms using the same basis in the second SLM. In each case, the modal power is measured, giving as a result a matrix that will reveal any mode crosstalk in the optical system (for a perfect system, this matrix should be an identity matrix). Figure 3(b) presents the measured crosstalk matrix for our system. Since it very closely resembles an identity matrix, we can conclude that the system is performing well and thus we can use it with our samples of interest.

IV. RESULTS

Even though the measurement of the step height only requires measuring the zeroth and first decomposition coefficients, we start by carrying out a complete modal decomposition of the sample with the idea of experimentally demonstrating our theoretical analysis. Figures 4(a) and 4(b) compare the experimental (left) and theoretical (right) results for $h = 0$ nm and $h = 60$ nm, respectively. Here, the modal power is encoded as color and the horizontal and vertical axes represent the added extra phase φ_{SLM} and the decomposing coefficient, respectively. It can be seen that the agreement between them is remarkable, confirming both the correctness and viability of our approach. Note how all even coefficients vanish and how the pattern in Fig. 4(b) is shifted to the right due to the finite height of the step. Figure 4(c) presents in detail an example of the data that we use to compute the height of one step. The measured modal powers of coefficients C_0 and C_1 are shown as solid squares, while the corresponding calculated y value as defined in Eq. (20) as hollow circles. The solid line represents the fitted curve [following the model in Eq. (21)], from which we determine $h = 58.8$ nm, which differs from the set value ($h_{set} = 60$ nm) only by 1.2 nm or about 2%.

Next, we vary the height of the step in the artificial sample from $h_{set} = 0$ nm to $h_{set} = 150$ nm in 15-nm intervals. In this case, we only measure 19 φ_{SLM} values per coefficient [instead of the 37 shown in Fig. 4(c)], which decreases the measurement time considerably. The calculated heights are presented in Fig. 4(d), with error bars given by the standard deviation for three repetitions. Remarkably, the differences between the set and calculated values are lower than 2 nm in all cases, as can be appreciated from the fact that all points fall in the close vicinity of the gray solid line, which depicts the ideal behavior, where the measured value is identical to the set one. We investigate the uncertainty in our measurement by repeating it 121 times for $h_{set} = 0$ nm. Figure 4(e) presents a histogram of the measured heights (bars) as well as its corresponding Gaussian fit (solid curve). From the latter, we determine a measured height of $h = 1.36$ nm with standard deviation $\sigma = 0.53$ nm, which is very close to the set value and comparable to typical uncertainties in measurements by scanning-force microscopes [9]. We point out, however, that this offset varies from measurement run to measurement run, but always in the $\pm$(1–2)-nm range. This is in the order of $\lambda/300$, whereas typical optical elements are in the order of $\lambda/10$. In other words, this offset is a tiny noise term that could easily arise from temperature fluctuations, small

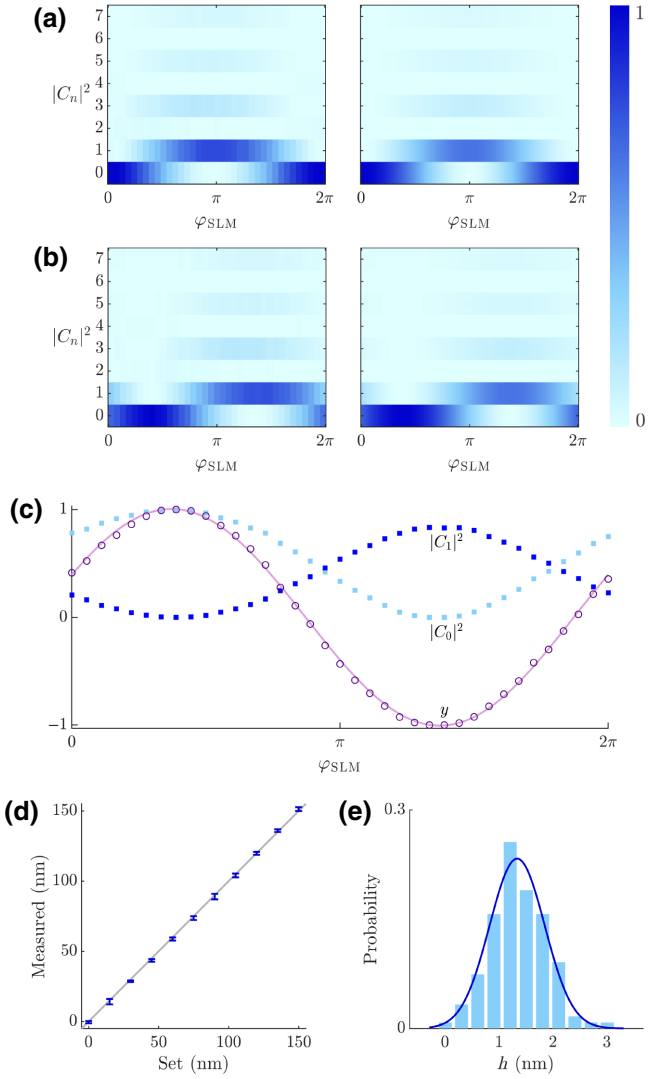

FIG. 4. A complete experimental (left) and analytical (right) modal decomposition for steps with height (a) $h = 0$ nm (a flat sample) and (b) $h = 60$ nm. As predicted by the theory, all even coefficients vanish and the zeroth and odd ones are shifted depending on the step height. (c) The first two measured coefficients (squares) and the corresponding computed y value [Eq. (20)] for $h = 60$ nm. The solid line shows the fitted curve from which we compute the measured height. (d) A comparison between the step-height set and measured values, with error bars representing the standard deviation from three measurements. An ideal case, where the two are identical, is shown as a continuous gray line along the diagonal. All calculated values are separated by less than 2 nm from the set values, demonstrating the good performance of the technique. (e) The histogram of 121 measured heights for $h = 0$ nm and the corresponding Gaussian fit, showing the small uncertainty in our method.

wave-front errors by marginal movement of the beam on optical elements, and so on.

Our digital version of the experiment allows us to easily test imperfections in real-world systems, e.g., surface

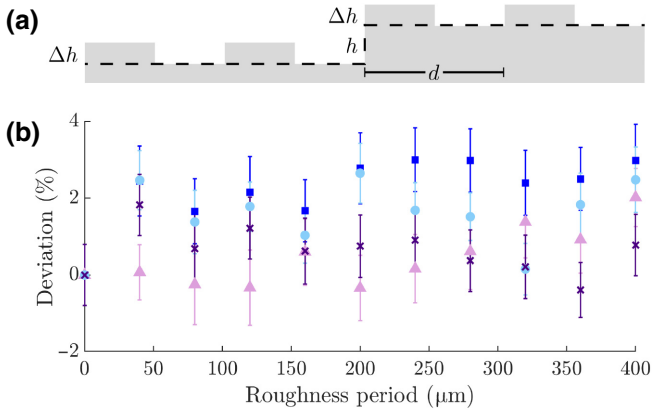

FIG. 5. (a) An illustration of the experimental simulation of surface roughness by a steplike function of high spatial frequency, defined by a roughness period, d. The dashed line represents a perfectly smooth step. (b) The deviation D of the measured value with roughness (h) from the value without (h_0), plotted as a function of the roughness period (d), for steps of height $h_{set} = 60$ nm. The triangles, squares, circles, and crosses represent data for roughness strengths $\Delta h = 1.61, 3.23, 4.84$, and 6.46 nm, respectively. For visualization purposes, (a) is not shown to scale.

roughness of samples. To this end, we introduce surface roughness as a periodic function of various heights and spatial frequency, as shown in Fig. 5(a). To quantify the effect on our step-height measurement, we deduce from the measurement the percentage deviation $D = 100\,(h - h_0/h_0)$ of the measured step height with (h) and without (h_0) roughness, plotted as a function of the roughness period (d) in Fig. 5(b). We program a step of height $h_{set} = 60$ nm and four values of roughness strength of depths $\Delta h = 1.61, 3.23, 4.84$, and 6.46 nm (corresponding to about 3, 5, 8, and 11% of the step height, respectively). Here, the markers represent the mean value and the error bars the standard error of ten repetitions and a zero value of the period represents a perfectly smooth step ($\Delta h = 0$ nm). The values that we use for both the roughness period and the strength are only limited by the physical pixel size and the modulation bit depth, respectively. Notably, the deviation shows a flat response as a function of the roughness period, with similar variation for the roughness depths: all are distributed in nearly the same range. This reinforces our conclusion that the offset error is dominated by random thermal or mechanical fluctuations and confirms that the approach correctly deduces the step height in the presence of roughness. As future work, we speculate that it may be possible to deduce the roughness itself by analyzing the higher-order HG modes.

V. DISCUSSION AND CONCLUSIONS

Although we only measure the height of the step, the approach has enough information to extract reflectivities

too, from the same fit. In our experience, a minimum of four points are required to make the fit reliable; thus it is enough to carry out eight measurements in total (four phase values for each decomposing coefficient C_0 and C_1), which is far less than we use in our proof-of-principle experiments (where we use 38 single measurements). In the event that no information about reflectivities is needed, this can be further reduced to four measurements in total, since is it enough to measure $|C_1|^2$. In addition, if it is preferable to avoid fitting, it is possible to simply scan over φ_{SLM} and compute the height from $h = (\varphi_{\max} - \pi)\lambda/4\pi$, where $\varphi_{\max}$ is the phase value for which the measured modal power is maximum.

Since our method is proposed as a single-point measurement, when using a sample with multiple steps, the height of each can be determined by moving the sample to locate each of them at the measurement point. In this case, the beam size must be small enough to ensure that the beam impinges solely onto one step at a time and the steps should be separated by at least twice the size of the minimum beam size of the optical system (imposed by its numerical aperture). Crucially, the precision of our method, and thus its longitudinal resolution, are limited only by the accuracy of the fitting, which in turns depends on the number of data points, the bit depth of the detector used, and the stability of the system. Strikingly somehow, measuring additional coefficients does not improve the precision. Instead, this can be accomplished by either increasing the number of phase values measured or repeating the complete measurement multiple times. One can understand this intuitively: the low-order HG mode is matched well to a step function, whereas higher-order terms are not. Rather, the faster spatial frequencies of the higher-order terms are themselves well matched to noise of similar spatial frequency; e.g., surface roughness.

Even though we present theory and experiments for reflective samples, our method can be easily adapted for transmissive ones. The working principle and procedure is the same, except that the phase factor in the model [Eq. (21)] is slightly different. In this case, the phase shift caused by the path difference between the two halves of the Gaussian beam is given by

$$\varphi_{\mathrm{step}} = \frac{2\pi n}{\lambda} h, \tag{22}$$

where n is the refractive index of the sample; thus the height of the step is computed from $h = \lambda/2\pi nB$. Interestingly, for transmissive samples, the measurement range varies as $\lambda/2n$, which for $n < 2$ is longer than for reflective samples.

In conclusion, modal decomposition expands a laser beam into its constituent modes (in some basis) and is routinely used for laser-beam analysis. Here, we alter this paradigm and outline theoretically and experimentally how it can be used to measure physical samples with sharp height differences. While many methods based on interference require the use of an optically flat sample as reference, our method does not need any type of experimental reference for calibration. Moreover, we present measurements within 2 nm from the known set values in all the measurement range, i.e., to within the noise of the experiment, thus demonstrating the excellent resolution of our approach. In addition, while in our experiments we use a liquid-crystal SLM for the modal analysis, this can be easily replaced by a digital micromirror device (DMD) for approximately 10 times faster and approximately 10 times cheaper deployment, without affecting the performance of the method [33]. Further, we point out that the approach requires only four single-point measurements to extract the power content of one of the two modes, from which full spatial resolution can be obtained. Thus, although we use a camera for these measurements, this can be replaced with simple photodiodes. This suggests that our accurate technique can be cost effective and fast, factors that are desirable for real-world applications.

ACKNOWLEDGMENTS

We thank Professor Enrique J. Galvez for allowing us to conduct additional experiments in his laboratory.

[1] R. Leach, C. Evans, L. He, A. Davies, A. Duparré, A. Henning, C. W. Jones, and D. O'Connor, Open questions in surface topography measurement: A roadmap, Surf. Topogr.: Metrology Prop. **3**, 013001 (2015).

[2] F. Fang, X. Zhang, W. Gao, Y. Guo, G. Byrne, and H. Hansen, Nanomanufacturing—perspective and applications, CIRP Ann. **66**, 683 (2017).

[3] U. Brand and W. Hillmann, Calibration of step height standards for nanometrology using interference microscopy and stylus profilometry, Precis. Eng. **17**, 22 (1995).

[4] G. Dai, L. Koenders, F. Pohlenz, T. Dziomba, and H.-U. Danzebrink, Accurate and traceable calibration of one-dimensional gratings, Meas. Sci. Technol. **16**, 1241 (2005).

[5] K. Sasagawa and J. Narita, Development of thin and flexible contact pressure sensing system for high spatial resolution measurements, Sens. Actuators A: Phys. **263**, 610 (2017).

[6] J. M. Bennett and J. H. Dancy, Stylus profiling instrument for measuring statistical properties of smooth optical surfaces, Appl. Opt. **20**, 1785 (1981).

[7] G. Binnig, H. Rohrer, C. Gerber, and E. Weibel, Surface Studies by Scanning Tunneling Microscopy, Phys. Rev. Lett. **49**, 57 (1982).

[8] G. Binnig, C. F. Quate, and C. Gerber, Atomic Force Microscope, Phys. Rev. Lett. **56**, 930 (1986).

[9] L. Koenders, P. Klapetek, F. Meli, and G. B. Picotto, Comparison on step height measurements in the nano and micrometre range by scanning force microscopes, Metrologia **43**, 04001 (2006).

[10] R. Leach, ed., *Optical Measurement of Surface Topography* (Springer, Berlin, 2011).
[11] Y. Tan, W. Wang, C. Xu, and S. Zhang, Laser confocal feedback tomography and nano-step height measurement, Sci. Rep. **3**, 2971 EP (2013).
[12] J. Wu, G. Ding, X. Chen, T. Han, X. Cai, L. Lei, and J. Wei, Nano step height measurement using an optical method, Sens. Actuators A: Phys. **257**, 92 (2017).
[13] A. G. Marrugo, F. Gao, and S. Zhang, State-of-the-art active optical techniques for three-dimensional surface metrology: A review, J. Opt. Soc. Am. A **37**, B60 (2020).
[14] K. Creath, Step height measurement using two-wavelength phase-shifting interferometry, Appl. Opt. **26**, 2810 (1987).
[15] H. J. Tiziani and H.-M. Uhde, Three-dimensional image sensing by chromatic confocal microscopy, Appl. Opt. **33**, 1838 (1994).
[16] M. C. Knauer, J. Kaminski, and G. Hausler, in *Optical Metrology in Production Engineering*, Vol. 5457, edited by W. Osten and M. Takeda, International Society for Optics and Photonics (SPIE, 2004), p. 366.
[17] L. Huang, M. Idir, C. Zuo, and A. Asundi, Review of phase measuring deflectometry, Opt. Lasers Eng. **107**, 247 (2018).
[18] M. K. Kim, Principles and techniques of digital holographic microscopy, SPIE Rev. **1**, 1 (2010).
[19] V. Rodríguez-Fajardo, C. Rosales-Guzmán, O. Mouane, D. Wamwangi, E. Sideras-Haddad, F. S. Roux, and A. Forbes, All-digital 3-dimensional profilometry of nano-scaled surfaces with spatial light modulators, Appl. Phys. B **127**, 145 (2021).
[20] P. de Groot, Principles of interference microscopy for the measurement of surface topography, Adv. Opt. Photon. **7**, 1 (2015).
[21] A. Forbes, M. de Oliveira, and M. R. Dennis, Structured light, Nat. Photonics **15**, 253 (2021).
[22] N. Hermosa, C. Rosales-Guzmán, S. F. Pereira, and J. P. Torres, Nanostep height measurement via spatial mode projection, Opt. Lett. **39**, 299 (2014).
[23] X. Dou, C. Min, Y. Zhang, S. F. Pereira, and X. Yuan, Optical singularity assisted method for accurate parameter detection of step-shaped nanostructure in coherent Fourier scatterometry, Opt. Express **30**, 29287 (2022).
[24] L. Torner, J. P. Torres, and S. Carrasco, Digital spiral imaging, Opt. Express **13**, 873 (2005).
[25] G. Molina-Terriza, L. Rebane, J. Torres, L. Torner, and S. Carrasco, Probing canonical geometrical objects by digital spiral imaging, J. Eur. Opt. Soc.—Rap. Publ. **2**, 07014 (2007).
[26] S. Fürhapter, A. Jesacher, S. Bernet, and M. Ritsch-Marte, Spiral phase contrast imaging in microscopy, Opt. Express **13**, 689 (2005).
[27] J. Pinnell, I. Nape, B. Sephton, M. A. Cox, V. Rodríguez-Fajardo, and A. Forbes, Modal analysis of structured light with spatial light modulators: A practical tutorial, J. Opt. Soc. Am. A **37**, C146 (2020).
[28] C. Rosales-Guzmán, N. Bhebhe, and A. Forbes, Multiplexing 200 modes on a single digital hologram, J. Opt. **25**, 25697 (2017).
[29] J. W. Goodman, *Introduction to Fourier Optics* (Roberts & Company, Greenwood Village, 2005), 3rd ed.
[30] I. S. Gradshteyn and I. M. Ryzhik, *Table of Integrals, Series, and Products*, edited by Daniel Zwillinger (Academic Press, Waltham, MA, 2015), 8th ed.
[31] E. Bolduc, N. Bent, E. Santamato, E. Karimi, and R. W. Boyd, Exact solution to simultaneous intensity and phase encryption with a single phase-only hologram, Opt. Lett. **38**, 3546 (2013).
[32] A. Jesacher, A. Schwaighofer, S. Fürhapter, C. Maurer, S. Bernet, and M. Ritsch-Marte, Wavefront correction of spatial light modulators using an optical vortex image, Opt. Express **15**, 5801 (2007).
[33] S. Scholes, R. Kara, J. Pinnell, V. Rodríguez-Fajardo, and A. Forbes, Structured light with digital micromirror devices: A guide to best practice, Opt. Eng. **59**, 1 (2019).